PCCP

ROYAL SOCIETY OF CHEMISTRY

PAPER

View Article Online
View Journal | View Issue

Cite this: *Phys. Chem. Chem. Phys.*, 2020, **22**, 25841

Adsorption, diffusion and aggregation of Ir atoms on graphdiyne: a first-principles investigation

Xin Liu, *[a] Meng Xu,[a] Yu Han *[b] and Changgong Meng *[a]

Received 2nd October 2020,
Accepted 26th October 2020

DOI: 10.1039/d0cp05197g

rsc.li/pccp

Graphdiyne (GDY) is a newly discovered 2D carbon allotrope, widely used as a support for heterogeneous transition metal catalysts. We investigated the binding, electronic structure, diffusion mechanisms and aggregation possibilities of mono-dispersed Ir atoms on GDY by extensive first-principles based calculations. The binding of Ir atoms on GDY can be up to −4.84 eV when the Ir atom is trapped in the C18 ring interacting with 2 adjacent diyne moieties connected to the same benzene ring. The diffusion of Ir atoms along the diyne moiety is quite facile with barriers less than 0.89 eV; the highest barrier for Ir diffusion into the C18 ring is 0.10 eV, whereas inter/intra-C18 ring diffusion is limited by a barrier of 1.64 eV, thereby leading to a dominant population of Ir atoms trapped in the C18 rings. The electronic structure of small Ir clusters was also investigated. Though the formation of Ir–Ir bonds is exothermic and thermodynamically favorable, which may, in some circumstances, even overwhelm the formation of interfacial Ir–C bonds, aggregation of Ir atoms into clusters is limited by the high energy barrier of inter/intra C18 ring diffusion. We propose that aggregation of Ir atoms into clusters may be initiated by shifting the diffusion thermodynamics deliberately and expect the finding may help to understand the stability and evolution of GDY based single atom catalysts.

1. Introduction

Supported noble metals, such as Pt, Pd, Ru, Rh, and Ir, are widely used heterogeneous catalysts that lower the energy and environment expense of chemical manufacture. To maximize the atomic utilization of precious noble metals, the concept of single atom catalysts (SACs) has been put forward, in which each individual under-coordinated metal atom acts as a reaction center.[1–4] In principle, the dispersion of metal atoms in a specific reaction condition is governed by the free-energy of the system, and is mainly contributed by the metal–support, metal–metal, metal–reactant interactions, *etc.* A suitable metal–support can suppress the aggregation of metal atoms and benefit the long term stability of the SACs,[5,6] whereas the detailed mechanism may vary with the nature of the metal and the support.[3,6] Therefore, it is of great significance to investigate the detailed binding, diffusion and aggregation of supported mono-dispersed noble metal atoms which are potential SACs.

Graphdiyne (GDY) is a newly discovered 2D carbon allotrope, which is composed of benzene rings (sp^2-C) interconnected by linear diyne moieties (sp-C) in a conjugated planar framework with uniform truncated triangle rings of 18 carbon atoms (C18). GDY is a middle-gap semiconductor with electron transfer rate of 1×10^4 cm^2 V^{-1} s^{-1},[7] while it has a large surface area[8] and superior chemical stability.[9–11] GDY has demonstrated great potential for significant applications in energy storage and conversion,[12–14] separation,[15] photo-electro detection,[10,16] and catalysis.[13,17–19] Many transition metal (*e.g.*, Cu,[20] Ru,[21] Pd,[22,23] Pt,[24,25] Ni and Fe[26]) SACs using GDY as the support have been reported for various chemical processes. Theoretical studies predicted that Ti and V SACs on GDY are good candidates for hydrogen evolution, while Pt and Ni SACs on GDY are effective for water splitting.[27] Currently, GDY based SACs are fabricated by wet chemical methods and their application is still hindered by the aggregation of metal species during reduction.[28,29] Therefore, it is of great significance to understand the evolution mechanism of metal species on GDY during the processing.

Iridium (Ir) is one of the most used noble metals in catalysis. The catalytic performances of Ir-based SACs on carbonaceous support have been well recognized in many chemical processes of industrial significance, such as oxidative conversion of ethane,[30] methanol carbonylation,[31] CO_2 hydrogenation,[32] nitrogen reduction,[33] *etc.* Ir_1/GDY was also predicted to be capable to catalyze CO oxidation.[34] Despite the research on Ir SACs, the potential applications of Ir atomic composites as magnetic materials, *etc.* were also explored before.[35–37] However, the stability and potential evolution of Ir single atoms on a specific support has yet to be systematically investigated

[a] *State Key Laboratory of Fine Chemicals, Department of Chemistry, School of Chemical Engineering, Dalian University of Technology, Dalian, 116024, P. R. China. E-mail: xliu@dlut.edu.cn, cgmeng@dlut.edu.cn*
[b] *KAUST Catalysis Center (KCC), King Abdullah University of Science and Technology, Thuwal 23955-6900, Saudi Arabia. E-mail: yu.han@kaust.edu.sa*

from a theoretical perspective. In this study, we investigated the binding, diffusion and aggregation of Ir single atoms on GDY by extensive first-principles based calculations. We focus on the detailed binding and diffusion mechanism and clustering possibilities and expect that these findings will help to understand the stability and evolution of GDY based SACs.

2. Theoretical methods

All the data presented were obtained from first-principles-based calculations with GGA-PBE functional and DSPP pseudopotential. These calculations were performed with DMol^3.[38–43] The structures were fully relaxed and the reaction potential energy surface were explored with linear and quadratic synchronous transit methods.[44,45] The binding structures and the transition states (TSs) were confirmed with the frequency analysis. Hirshfeld method was used in the population analysis.[46] The convergence criteria for energy, gradient, displacement and density are 1×10^{-5} a.u., 2.00×10^{-3} Å, 5.00×10^{-3} Å and 1×10^{-6} a.u., respectively. With the theoretical approach, the lattice parameters of Ir and GDY are calculated as 3.89 and 9.47 Å, respectively.[47,48]

3. Results and discussions

3.1 The binding of mono-dispersed Ir atoms to GDY

The pristine GDY is comprised by C1, C2 and C3 and their symmetrically equivalent atoms (one group was named C1′, C2′ and C3′, Fig. 1). C2 and C3 are sp-C, together with their equivalent atoms form the diyne moieties, connecting with the benzene moieties comprised by C1 and equivalent atoms into the GDY framework. The calculated C1–C1′, C1–C2, C2–C3 and C3–C4 distances are 1.43, 1.40, 1.24 and 1.34 Å, respectively and the bulk bandgap is 0.45 eV (Fig. 2).[49–51] For pristine GDY, the Density of States (DOS) peaks in [−6.0, −10.0] eV are contributed by C1, the peaks in [−5.0, −2.0] eV are comprised by C3 states and the interactions between C2 and C3, while those in [−2.0, 0.0] eV mainly correspond to C2 states (Fig. 2a).

We started with the binding of mono-dispersed Ir atoms onto GDY (Fig. 1). The most plausible deposition structure of Ir over GDY is H2 (Fig. 1b), where Ir atom lies in a corner of the C18 ring, on the bisector of 2 adjacent diyne moieties and interacts with 4 nearest neighboring sp-C atoms (C2, C3, C2′ and C3′ in Fig. 1a and 2a) and the calculated E_b with and without consideration of van de Waals interaction are −4.93 and −4.84 eV, respectively. As van de Waals interaction only plays a minor role (0.09 eV) in E_b, it was not considered further.[52] The calculated E_b is in reasonable agreement with the reported values for Ir on GDY and graphyne.[34,53] In H2, Ir–C2/C2′ and Ir–C3/C3′ distances are 1.96 and 2.06 Å, respectively, and C1–C1′, C1–C2, C2–C3 and C3–C4 distances are elongated to 1.44, 1.42, 1.33 and 1.35 Å, respectively, suggesting the formation of Ir–C bonds and the alternation of the conjugation in GDY (Fig. 1b and 2b). This is in agreement with the calculated isosurface plot charge density difference in Fig. 2b. DOS analysis also proofs that, due to the Ir–C interactions, the peaks of Ir–sp and Ir–d resonance strongly with that of C states in [−5.0, −3.5] eV and [−1.0, 0] eV, corresponding to the alternation of the conjugation among C atoms and the formation of Ir–C2/C3 interactions (Fig. 2a). The difference in the Ir–C2 and Ir–C3 distances can be attributed to local structure of GDY.

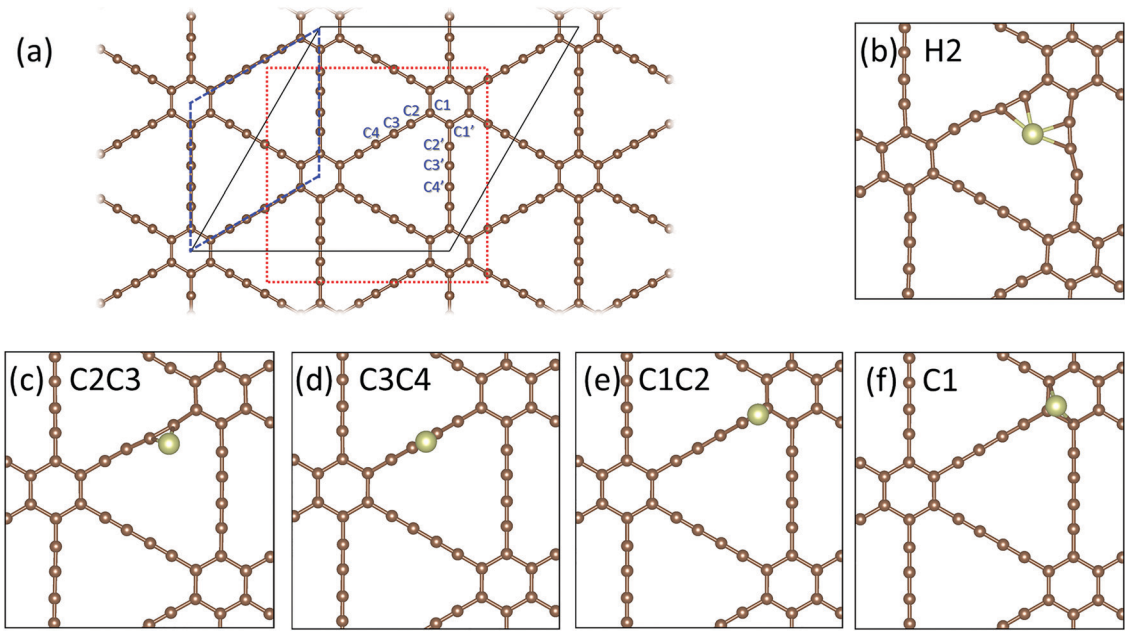

Fig. 1 Schematic view of the GDY model (a) and the calculated binding structures of Ir atom on GDY, namely H2 (b), C2C3 (c), C3C4 (d), C1C2 (e) and C1 (f). The (1 × 1) and ($\sqrt{3} \times \sqrt{3}$) cells used for the calculation and the view point in (b–f) are highlighted with blue, black and red (dashed) lines, respectively and the nomenclature of the binding structures of the C atoms are also marked in blue. In (a), C3 and C4 are equivalent, C3′ and C4′ are also equivalent. In (a–f) the Ir and C atoms are in brown and dark yellow, respectively.

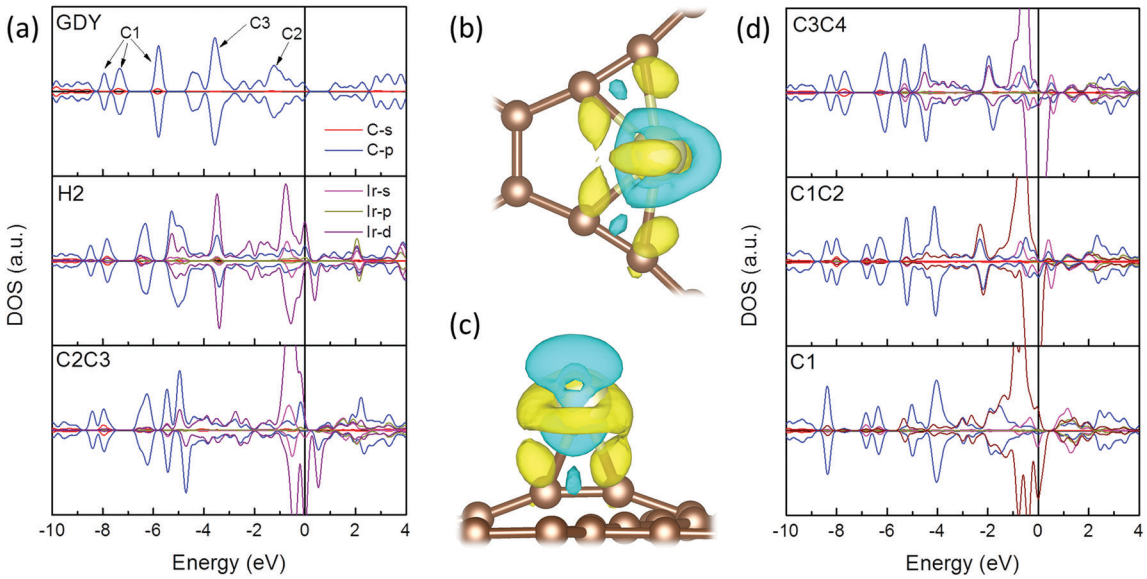

Fig. 2 Projected DOS of pristine GDY, H2 and C2C3 (a), isosurface plot of differential charge density for Ir deposition at H2 (b) and C2C3 (c) and projected DOS of C3C4, C1C2 and C1 (d). In (b and c), the charge accumulation and depletion regions are in yellow and blue, respectively and the isovalues are $\pm 2 \times 10^{-6}$ a.u., respectively. In (b and c), the C and Ir atoms are in brown and dark yellow, respectively.

There are also other Ir deposition structures (Fig. 1a) due to the mixed sp and sp^2 hybridization in GDY. Rotation of Ir along one of the diyne moiety (C2C3C4) from the H2 leads to breaking of the Ir–C bonds to another diyne moiety (C2′C3′C4′). In the resulting structure (C2C3, Fig. 1c), Ir stands immediately on the middle of 2 sp-C, with the Ir–C2 and Ir–C3 distances shortened to 1.92 and 1.95 Å, respectively. The charge transfer at the Ir–GDY interface (Fig. 2c) leads to elongation of C2–C3 distance to 1.35 Å and Ir atom extends above the GDY lattice. The DOS of C2C3 is similar to that of H2, except that both peaks in [−5.0, −4.0] eV corresponding to C3 and the interaction among C atoms were downshifted to ∼−5 eV to resonance with Ir states (Fig. 2a). The breaking of Ir–C2′ and Ir–C3′ bonds and strengthening of Ir–C2 and Ir–C3 bonds makes E_b at C2C3 −3.23 eV and is 1.61 eV less stable than that at H2.

Ir may further shift from C2C3 in direction of C4 that is symmetrically equivalent to C3 for formation of C3C4 (Fig. 1d) or to the benzene ring to form C1C2 (Fig. 1e). In C3C4 (E_b = −2.46 eV, Fig. 1d), the Ir–C distances are both 1.98 Å and the 2 sp-C interacting directly with Ir are also connected *via* acetylene bonds to other C atoms. Interactions among Ir states of t_2 or t_{2g} symmetry and the GDY π/π* states are allowed and lead to further alternation of the hybridization within GDY. This is in agreement with the strong resonance of DOS peaks of C3 and Ir–d states at ∼−4 eV and in [−2.0, 0] eV (Fig. 2d). The case of C1C2 (Fig. 1e, E_b = −2.48 eV) is similar to C3C4, considering the bonding between C1(sp^2-C) and C2(sp-C). In C1C2, the Ir–C1 and Ir–C2 distances are 2.08 and 1.94 Å, respectively. The split of DOS peaks of C1 and the resonance of Ir and C states right below −2 eV (Fig. 2d) confirms alternation of the conjugation among C atoms. The deposition of Ir on the benzene moiety (C1, E_b = −2.38 eV, Fig. 1f) is the least plausible among the deposition structures considered. In C1, Ir atom interacts with 3 adjacent sp^2-C atoms on the benzene ring at Ir–C distances of 2.02, 2.15 and 2.15 Å, respectively. Correspondingly, DOS peaks of C1 at ∼−6 eV are split below −6 eV and strong resonance of C and Ir states can also be observed in [−2.0, 0] eV (Fig. 2d). The binding of Ir on top of the center of benzene ring or on the edge of benzene ring were also investigated, but the structures will evolve to either C1 or H2 during structure optimization, and they were not considered further.

The E_b of Ir deposition on GDY falls in the middle of the E_b on pristine graphene and defective graphene, which are −1.74 and −9.80 eV, respectively. Mi *et al.* also reported the E_b of −4.66 and −8.13 eV for Ir atomic deposition on pristine and defective WSe_2.[35,36] Considering the calculated E_b of −4.84 eV, GDY may provide anchor sites for Ir atoms. The difference in E_b can be attributed to the nature of Ir–support bonding, while Ir is stabilized by d–π/π* coordination with sp-C on GDY.[35–37] The deposition of Ir atoms also induces strong charge transfer at the interface, from Ir to the C atoms of GDY (Fig. 2b and c). Depending on the detailed the deposition structures, the calculated charge on Ir atom are +0.17, +0.10, +0.14, +0.15 and +0.18 $|e|$ for H2, C2C3, C3C4, C1C2 and C1, respectively. Ir atoms are not fully coordinated in all these deposition structures and interact with only adjacent C atoms. The sharp spikes of Ir–d states on DOS at the Fermi level (Fig. 2a and d) suggest that these positively charged Ir atoms would be highly reactive to approaching species, such as CO, NO, C_2H_4, *etc.*[34] and may prefer to bind species through σ–π coordination, rather than by charge transfer with strong electron withdrawing species, such as O_2, *etc.*[54,55]

3.2 Diffusion of Ir atom on GDY

According to the calculated E_b, the exothermicity for Ir diffusion along the GDY framework (from C1 to C3C4) would be less than 0.75 eV, while this would increase to ∼2.46 eV when H2 is

considered. As it is directly related to the stability and aggregation possibility of mono-dispersed Ir atoms, the Ir diffusion among these local minima on GDY was investigated (Fig. 3). The potential Ir diffusion paths can be classified into 3 kinds, namely the Ir atomic diffusion along the GDY framework, from GDY framework to H2, and inter and intra-C18 ring diffusion of Ir from H2.

The Ir atomic diffusion along the GDY framework between adjacent sites was investigated first (Fig. 3a, upper panel). The diffusion of Ir from C1 to C1C2 is exothermic by 0.10 eV and the calculated energy barrier is 0.20 eV. In the optimized TS ($TS_{C1-C1C2}$, Fig. 3b), Ir moves slightly to stand right above C1 atom forming a "Jingle bell" like structure at Ir–C1, Ir–C1′, Ir–C2 distances of 1.98, 2.22 and 2.29 Å, respectively, with an imaginary frequency of -162 cm^{-1} corresponding to the C2 out-of-plane vibration mode approaching to Ir. Ir may further diffuse to C2C3 that is adjacent to C1C2. The diffusion is 0.75 eV exothermic with an energy barrier of 0.18 eV. In TS $_{C1C2-C2C3}$ (Fig. 3b), Ir stands immediately on top of C2 and the Ir–C2, Ir–C3, Ir–C1 distances are 1.89, 2.61 and 2.38 Å, respectively and the calculated imaginary frequency is -115 cm^{-1}, corresponding to C3 approaching to and C1 leaving from Ir. From C2C3, Ir may further move to C3C4 by passing the TS $_{C2C3-C3C4}$ (Fig. 3c). Ir diffusion in this way is 0.77 eV endothermic and the energy barrier is 0.89 eV, and this endothermicity can be attributed to the difference in Ir–C bonding at C2C3 and C3C4. The imaginary frequency is -204 cm^{-1}, corresponding to attaching of C4 to and leaving of C2 from Ir. According to the calculated barriers, Ir diffusion along the GDY framework would be rather facile with diffusion barriers less than 1.0 eV. Previously, a diffusion barrier of 0.35 eV for Ir on pristine graphene was reported, in reasonable agreement with the current result.[37,56] The diffusion from C1C2 and C3C4 to C2C3 is facile with barriers less than 0.20 eV while the barriers for reverse diffusion are all $\sim$0.80 eV. A close inspection of the TS structures show that Ir diffusion is actually facilitated by asymmetrical vibration modes of GDY framework, through the approaching and leaving of C atoms adjacent to Ir.

As H2 is the most plausible deposition structure, the diffusion from C1, C1C2, C2C3 and C3C4 to H2 was also investigated. The diffusion from C1 to H2 requires breaking the Ir–C1 bonds, so the calculated barrier is 0.10 eV and the diffusion is 2.46 eV exothermic. In TS_{C1-H2} (Fig. 3e), Ir stands in the middle of C1 and C1′. The imaginary frequency is -41 cm^{-1}, corresponding to Ir motion to interact with only C1 and C1′. As for Ir diffusion from C1C2 to H2, it is 2.37 eV exothermic with a barrier of 0.01 eV. In $TS_{C1C2-H2}$ (Fig. 3f), Ir–C1 and Ir–C2 distances are 2.07 and 1.94 Å, respectively. The imaginary frequency is -67 cm^{-1}, associated with the Ir vibration in the direction of C2′ and C3′. Ir diffusion from C2C3 to H2 is 1.61 eV exothermic and the barrier is 0.03 eV. In TS $_{C2C3-H2}$ (Fig. 3g), Ir is stretching to reach C2′C3′ for formation of H2 at an imaginary frequency of -86 cm^{-1}. We also tried to find the TS for Ir diffusion from C3C4 to H2, but found it exactly the same as TS $_{C2C3-H2}$. Considering the reverse barrier for TS $_{C2C3-C3C4}$ is as low as 0.12 eV, Ir may diffuse to C2C3 first and

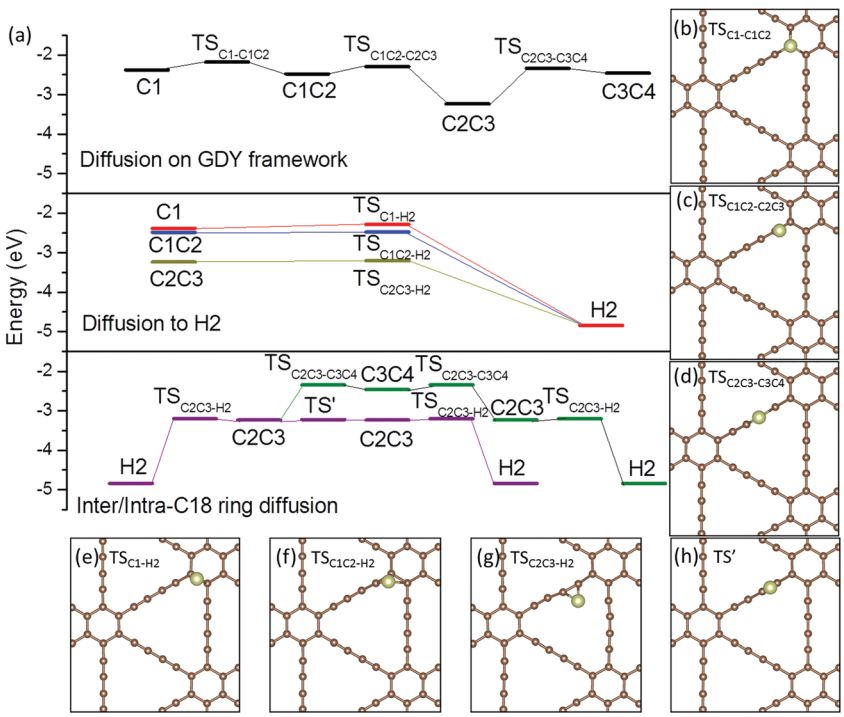

Fig. 3 The Ir diffusion potential surface on GDY (a) and structures of transition states involved, namely $TS_{C1-C1C2}$ (b), $TS_{C1C2-C2C3}$ (c), $TS_{C2C3-C3C4}$ (d), TS_{C1-H2} (e), $TS_{C1C2-H2}$ (f), $TS_{C2C3-H2}$ (g) and TS′(h). In (a), the energy are given with respect to pristine GDY and Ir atom. In lower panel of (a), the potential energy surface for the inter-C18 ring diffusion is in purple while that for the intra-C18 ring diffusion is in dark green. In (b–h), the C and Ir atoms are in brown and dark yellow, respectively.

then fall into H2. According to the calculated diffusion barriers and E_b, the Ir diffusion to H2 is thermodynamic driven and is exothermic by at least 1.64 eV (from C2C3 to H2). In this sense, the deposited Ir may diffuse either along the GDY framework to reach adjacent C2C3 and then fall into the well of H2, or diffuse directly into neighboring H2. The lifetime of Ir at H2 is 2.16×10^{10} s, as estimated by $\tau = (h/k_BT)\exp(E/k_BT)$, where k_B, h and E are the Boltzmann constant, Planck constant and energy barrier for Ir diffusion from H2. Therefore, a dominate population of Ir atoms will be trapped at H2.

Based on the aforementioned diffusion paths and barriers, the intra-C18 ring diffusion from H2 to another site equivalent was also deduced. Ir at H2 may go through $TS_{C2C3-H2}$ with a reverse barrier of 1.64 eV and an endothermicity of 1.61 eV to reach C2C3. It then goes energy uphill ($TS_{C2C3-C3C4}$) at a barrier of 0.89 eV and then goes downhill ($TS_{C2C3-C3C4}$) through C3C4 to reach the site equivalent to C2C3 at a barrier of 0.12 eV and finally falls into another equivalent H2 on the same C18 ring with a negligible barrier of 0.03 eV. It is apparent that this process is limited by $TS_{H2-C2C3}$. The mechanism for Ir inter-C18 ring diffusion was also deduced. In C2C3, Ir is extending out to the direction of C2′C3′ (Fig. 1a and 3g). As a diyne moiety is actually a C_2 axis in GDY lattice, there is another Ir deposition structure equivalent to C2C3 with Ir extending to another adjacent diyne moiety attached to the same benzene ring. The TS (TS′, Fig. 3h) between these 2 C2C3 structures corresponds to Ir inter-C18 ring diffusion among adjacent rings and the calculated reaction barrier is only 0.02 eV. This, together with the barriers for $TS_{C2C3-H2}$ and $TS_{H2-C2C3}$ which are 0.01 and 1.64 eV, respectively, suggests that Ir inter-C18 ring diffusion is also limited by $TS_{H2-C2C3}$. Comparing with the barriers for Ir diffusion along the GDY framework, intra and inter C18-rings, deposited Ir will be trapped at H2 and diffuse to adjacent H2 by inter or intra C18-ring diffusion with barriers of 1.64 eV.

3.3 The thermodynamic for Ir_n (n = 2, 3, 4) formation on GDY

The deposition of Ir_n (n = 2, 3, 4) cluster was also investigated to deduce the driving force for potential aggregation of monodispersed Ir on GDY (Fig. 4). Among the considered Ir_2/GDY structures, 2 Ir stand in 2 adjacent H2 sites on the same C18 ring is the most plausible (Fig. 4a). In this structure, one of the neighboring diyne moieties is deformed to accommodate Ir_2. The minimum and maximum Ir–C distances are 2.00 and 2.48 Å, respectively. The Ir–Ir distance of 2.48 Å is already much shorter than that in bulk Ir (2.75 Å), suggesting the bonding between 2 Ir atoms. The calculated E_b is −10.56 eV, equivalent to −5.28 eV/Ir, and is 0.44 eV more plausible than that for H2 (Fig. 1b). Similarly, the calculated E_b for Ir_3/GDY and Ir_4/GDY (Fig. 4b and c) are −16.12 and −20.37 eV, respectively and the E_b averaged over Ir atoms are −5.37 and −5.09 eV/Ir, respectively. In the most plausible structure of Ir_3/GDY, 3 Ir atoms are in a distorted planar structure with Ir–Ir distances of 2.54, 2.75 and 2.72 Å, respectively to interact with C atoms on the same C18 ring. Similar Pt_3, Pd_3 and Ni_3/GDY structures were also reported stable by Li and Xiao *et al.* even in electrochemical leaching environments.[29] However, the case of Ir_4/GDY is different from Ir_2 and Ir_3/GDY. In Ir_4/GDY, 4 Ir atoms form a tetrahedral with 3 Ir atoms in a planar structure, right above the C18 ring of GDY and the 4th Ir atom on the top at Ir–Ir distances of 2.54 Å. By correlating the interfacial Ir–C bonds in

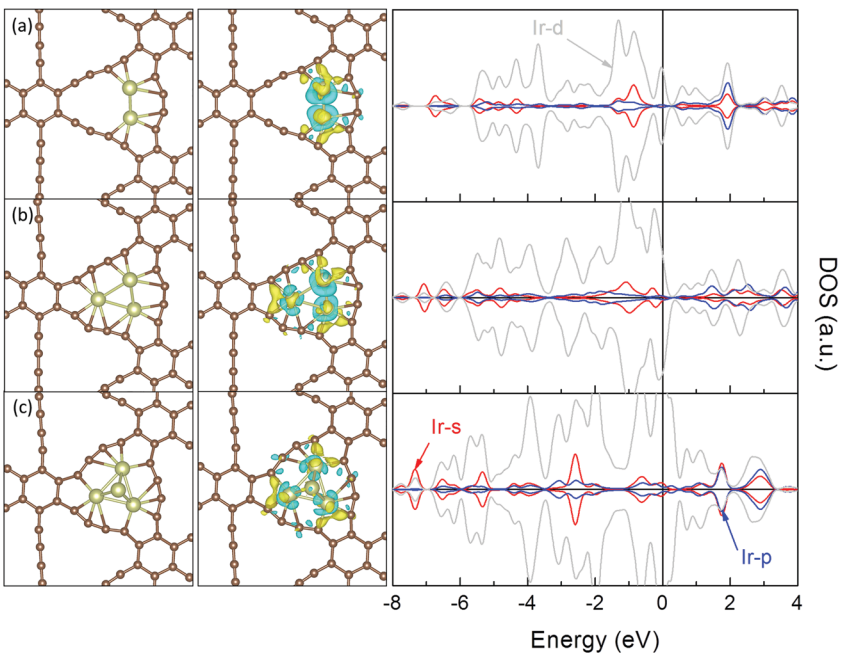

Fig. 4 The most plausible structures (left panel) of Ir_2/GDY (a), Ir_3/GDY (b) and Ir_4/GDY (c), the isosurface plots (middle panel) of corresponding charge density difference calculated as $\Delta\rho = \rho_{Ir_n/GDY} - \rho_{Ir_n} - \rho_{GDY}$ and the projected DOS of Ir_n in Ir_n/GDY. In the left and middle panels, the C and Ir atoms are in brown and dark yellow, respectively. The charge depletion and accumulation regions are in blue and yellow, respectively and the isovalue is $\pm 2 \times 10^{-6}$ a.u.

Ir_3/GDY and Ir_4/GDY with the calculated E_b, it is apparent that Ir–Ir bonds also contribute to the formation of deposited Ir clusters, and aggregation of Ir atoms would be thermodynamics driven. Considering the diffusion of Ir atoms on GDY is limited by $TS_{H2–C2C3}$ with a barrier of 1.64 eV, lower this barrier deliberately may lead to aggregation of Ir atoms into clusters driven by the thermodynamics of Ir–Ir bond formation. In this sense, the observed aggregation of metal species on GDY can only be attributed to other factors, such as the involvement of reaction species during post-synthesis processing, *etc.*, which may alter the free energy of the metal species as well as the thermodynamics drastically.[6,28]

The deposition of Ir clusters on GDY is accompanied with charge transfer from the cluster to the GDY substrate. The total charge on Ir cluster in Ir_2/GDY, Ir_3/GDY and Ir_4/GDY are +0.24, +0.25 and +0.30 $|e|$, respectively with respect to neutral Ir atoms (Fig. 4, middle panel) and the charge accumulation regions are always localized around the C atoms adjacent to Ir in the direction Ir–C bonds (Fig. 4, middle panel). Compared with the DOS of H2 (Fig. 2a), the DOS peaks of supported Ir clusters are downshifted and broadened in the range $[-6.0, 0]$ eV providing evidence for the hybridization among states of Ir and adjacent C atoms. There is always a peak of Ir-d state at the Fermi level (Fig. 4, right panel), suggesting the high reactivity of these supported clusters, similar to mono-dispersed Ir atoms, to approaching molecules for their activation and conversion.[30,32,54,55]

4. Conclusions

The electronic structure, binding, diffusion mechanisms and aggregation possibilities of mono-dispersed Ir atom on GDY by extensive first-principles based calculations. The binding of Ir atoms on GDY can be up to −4.84 eV when the Ir atom in trapped in C18 ring interacting with 2 adjacent diyne moieties connected to the same benzene ring. The diffusion of Ir along the diyne moiety is quite facile with barriers less than 0.89 eV and the highest barrier for Ir diffusion into the C18 ring is 0.10 eV, leading to a high population of Ir atoms trapped in the C18 ring. The barriers for inter/intra-C18 ring diffusion are 1.64 eV and may limit further diffusion of Ir atoms. The formation of small Ir cluster is thermodynamics driven due to the exothermic formation of Ir–Ir bonds which may in some circumstances even overwhelm the formation of interfacial Ir–C bonds. However, the aggregation of Ir atoms into clusters is limited by the outward diffusion from the C18 ring with a barrier of 1.64 eV, in vacuum. We propose that aggregation of Ir atoms into clusters may be initiated by shifting the diffusion thermodynamics deliberately, by interaction with organic substrates, *etc.*, and expect the finding will help to understand the stability and evolution of GDY based SACs.

Author contributions

X. L. conceived the research, performed the calculations, analyzed the results and drafted the manuscript. X. L. discussed results with Y. H. and C. M. Y. H. and C. M. commented the results and read the manuscript. All authors have given approval to the final version of the manuscript.

Conflicts of interest

There are no conflicts to declare.

Acknowledgements

This work was supported by NSFC (21771029, 21771030, 21373036, 11811530631, 21573034, and 21103015). The supercomputer time was supported by the High Performance Computing Center at Dalian University of Technology, National Supercomputing Center in Guangzhou, China and Supercomputing Core Laboratory at King Abdullah University of Science & Technology.

References

1 B. T. Qiao, J. X. Liang, A. Q. Wang, C. Q. Xu, J. Li, T. Zhang and J. Y. Liu, *Nano Res.*, 2015, **8**, 2913–2924.
2 J. Y. Liu, *ACS Catal.*, 2017, **7**, 34–59.
3 A. Q. Wang, J. Li and T. Zhang, *Nat. Rev. Chem.*, 2018, **2**, 65–81.
4 X. F. Yang, A. Q. Wang, B. T. Qiao, J. Li, J. Y. Liu and T. Zhang, *Acc. Chem. Res.*, 2013, **46**, 1740–1748.
5 J. C. Liu, Y. Tang, Y. G. Wang, T. Zhang and J. Li, *Natl. Sci. Rev.*, 2018, **5**, 638–641.
6 R. H. Ouyang, J. X. Liu and W. X. Li, *J. Am. Chem. Soc.*, 2013, **135**, 1760–1771.
7 A. L. Ivanovskii, *Prog. Solid State Chem.*, 2013, **41**, 1–19.
8 C. Lu, Y. Yang, J. Wang, R. P. Fu, X. X. Zhao, L. Zhao, Y. Ming, Y. Hu, H. Z. Lin, X. M. Tao, Y. L. Li and W. Chen, *Nat. Commun.*, 2018, **9**, 752.
9 X. Gao, H. B. Liu, D. Wang and J. Zhang, *Chem. Soc. Rev.*, 2019, **48**, 908–936.
10 Y. S. Zhao, H. J. Tang, N. L. Yang and D. Wang, *Adv. Sci.*, 2018, **5**, 1800959.
11 Y. J. Li, L. Xu, H. B. Liu and Y. L. Li, *Chem. Soc. Rev.*, 2014, **43**, 2572–2586.
12 N. Wang, J. J. He, K. Wang, Y. J. Zhao, T. G. Jiu, C. S. Huang and Y. L. Li, *Adv. Mater.*, 2019, **31**, 1803202.
13 J. Li, X. Gao, L. Zhu, M. N. Ghazzal, J. Zhang, C. H. Tung and L. Z. Wu, *Energy Environ. Sci.*, 2020, **13**, 1326–1346.
14 Z. C. Zuo and Y. L. Li, *Joule*, 2019, **3**, 899–903.
15 X. Gao, J. Y. Zhou, R. Du, Z. Q. Xie, S. B. Deng, R. Liu, Z. F. Liu and J. Zhang, *Adv. Mater.*, 2016, **28**, 168–173.
16 J. Li, X. Gao, B. Liu, Q. L. Feng, X. B. Li, M. Y. Huang, Z. F. Liu, J. Zhang, C. H. Tung and L. Z. Wu, *J. Am. Chem. Soc.*, 2016, **138**, 3954–3957.
17 J. Li, X. Gao, X. Jiang, X. B. Li, Z. F. Liu, J. Zhang, C. H. Tung and L. Z. Wu, *ACS Catal.*, 2017, **7**, 5209–5213.
18 Y. Gao, Z. W. Cai, X. C. Wu, Z. L. Lv, P. Wu and C. X. Cai, *ACS Catal.*, 2018, **8**, 10364–10374.

19 Y. Fang, Y. R. Xue, Y. J. Li, H. D. Yu, L. Hui, Y. X. Liu, C. Y. Xing, C. Zhang, D. Y. Zhang, Z. Q. Wang, X. Chen, Y. Gao, B. L. Huang and Y. L. Li, *Angew. Chem., Int. Ed.*, 2020, **59**, 13021–13027.
20 L. Hui, Y. Xue, H. Yu, C. Zhang, B. Huang and Y. Li, *ChemPhysChem*, 2020, **21**, 2145–2149.
21 B. Z. Lu, L. Guo, F. Wu, Y. Peng, J. E. Lu, T. J. Smart, N. Wang, Y. Z. Finfrock, D. Morris, P. Zhang, N. Li, P. Gao, Y. Ping and S. W. Chen, *Nat. Commun.*, 2019, **10**, 631.
22 H. T. Qi, P. Yu, Y. X. Wang, G. C. Han, H. B. Liu, Y. P. Yi, Y. L. Li and L. Q. Mao, *J. Am. Chem. Soc.*, 2015, **137**, 5260–5263.
23 H. D. Yu, Y. R. Xue, B. L. Huang, L. Hui, C. Zhang, Y. Fang, Y. X. Liu, Y. J. Zhao, Y. J. Li, H. B. Liu and Y. L. Li, *iScience*, 2019, **11**, 31–41.
24 H. H. Wei, K. Huang, D. Wang, R. Y. Zhang, B. H. Ge, J. Y. Ma, B. Wen, S. Zhang, Q. Y. Li, M. Lei, C. Zhang, J. Irawan, L. M. Liu and H. Wu, *Nat. Commun.*, 2017, **8**, 8.
25 X. P. Yin, H. J. Wang, S. F. Tang, X. L. Lu, M. Shu, R. Si and T. B. Lu, *Angew. Chem., Int. Ed.*, 2018, **57**, 9382–9386.
26 Y. R. Xue, B. L. Huang, Y. P. Yi, Y. Guo, Z. C. Zuo, Y. J. Li, Z. Y. Jia, H. B. Liu and Y. L. Li, *Nat. Commun.*, 2018, **9**, 10.
27 T. W. He, S. K. Matta, G. Will and A. J. Du, *Small Methods*, 2019, **3**, 1800419.
28 J. Q. Li and J. Zhang, *Chinese Science Bulletin-Chinese*, 2019, **64**, 3649–3664.
29 J. C. Liu, H. Xiao and J. Li, *J. Am. Chem. Soc.*, 2020, **142**, 3375–3383.
30 R. X. Jin, M. Peng, A. Li, Y. C. Deng, Z. M. Jia, F. Huang, Y. J. Ling, F. Yang, H. Fu, J. L. Xie, X. D. Hang, D. Q. Xiao, Z. Jiang, H. Y. Liu and D. Ma, *J. Am. Chem. Soc.*, 2019, **141**, 18921–18925.
31 S. Q. Peng, X. S. Lin, X. G. Song, Y. Liu, Z. Jiang, P. Hemberger, A. Bodi and Y. J. Ding, *J. Catal.*, 2020, **381**, 193–203.
32 X. Z. Shao, X. F. Yang, J. M. Xu, S. Liu, S. Miao, X. Y. Liu, X. Su, H. M. Duan, Y. Q. Huang and T. Zhang, *Chem*, 2019, **5**, 693–705.
33 X. Y. Guo, J. X. Gu, S. R. Lin, S. L. Zhang, Z. F. Chen and S. P. Huang, *J. Am. Chem. Soc.*, 2020, **142**, 5709–5721.
34 G. L. Xu, R. Wang, Y. C. Ding, Z. S. Lu, D. W. Ma and Z. X. Yang, *J. Phys. Chem. C*, 2018, **122**, 23481–23492.
35 Y. Song, X. C. Wang and W. B. Mi, *Phys. Rev. Mater.*, 2017, **1**, 5.
36 C. Zhang, X. C. Wang and W. B. Mi, *J. Mater. Chem. C*, 2020, **8**, 11417–11425.
37 Y. Han, G. X. Ge, J. G. Wan, J. J. Zhao, F. Q. Song and G. H. Wang, *Phys. Rev. B: Condens. Matter Mater. Phys.*, 2013, **87**, 155408.
38 B. Delley, *J. Chem. Phys.*, 1990, **92**, 508–517.
39 B. Delley, *J. Chem. Phys.*, 2000, **113**, 7756–7764.
40 J. P. Perdew, K. Burke and M. Ernzerhof, *Phys. Rev. Lett.*, 1996, **77**, 3865–3868.
41 B. Delley, *Phys. Rev. B: Condens. Matter Mater. Phys.*, 2002, **66**, 155125.
42 D. Rappoport, N. R. M. Crawford, F. Furche and K. Burke, in *Encyclopedia of Inorganic Chemistry*, John Wiley & Sons, Ltd, 2006, pp. 1–14, DOI: 10.1002/0470862106.ia615.
43 Y. Inada and H. Orita, *J. Comput. Chem.*, 2008, **29**, 225–232.
44 N. Govind, M. Petersen, G. Fitzgerald, D. King-Smith and J. Andzelm, *Comput. Mater. Sci.*, 2003, **28**, 250–258.
45 H. J. Monkhorst and J. D. Pack, *Phys. Rev. B: Solid State*, 1976, **13**, 5188–5192.
46 F. L. Hirshfeld, *Theor. Chim. Acta*, 1977, **44**, 129–138.
47 M. Gajdos, A. Eichler and J. Hafner, *J. Phys.: Condens. Matter*, 2004, **16**, 1141–1164.
48 Q. Yue, S. L. Chang, J. Kang, S. Q. Qin and J. B. Li, *J. Phys. Chem. C*, 2013, **117**, 14804–14811.
49 J. Zhou, K. Lv, Q. Wang, X. S. Chen, Q. Sun and P. Jena, *J. Chem. Phys.*, 2011, **134**, 174701.
50 N. Narita, S. Nagai, S. Suzuki and K. Nakao, *Phys. Rev. B: Solid State*, 1998, **58**, 11009–11014.
51 N. Ketabi, T. M. Tolhurst, B. Leedahl, H. B. Liu, Y. L. Li and A. Moewes, *Carbon*, 2017, **123**, 1–6.
52 E. R. McNellis, J. Meyer and K. Reuter, *Phys. Rev. B: Condens. Matter Mater. Phys.*, 2009, **80**, 205414.
53 D. W. Ma, T. X. Li, Q. G. Wang, G. Yang, C. Z. He, B. Y. Ma and Z. S. Lu, *Carbon*, 2015, **95**, 756–765.
54 X. Liu, M. Xu, L. Wan, H. Zhu, K. Yao, R. Linguerri, G. Chambaud, Y. Han and C. Meng, *ACS Catal.*, 2020, **10**, 3084–3093.
55 X. Liu, H. Zhu, R. Linguerri, Y. Han, G. Chambaud and C. Meng, *ChemistrySelect*, 2017, **2**, 9412–9419.
56 Q. Tang, Z. Zhou and Z. F. Chen, *Nanoscale*, 2013, **5**, 4541–4583.